Thermal transport and irreversibility in rotating MHD hybrid nanofluid flow under the Cattaneo–Christov heat flux model

The present study investigates the combined effects of thermal relaxation and magnetic field on the transport characteristics of an electrically conducting fluid using the modified Fourier law, namely the Cattaneo–Christov heat-flux model. Unlike the classical Fourier formulation, the proposed model accounts for finite thermal propagation speed and eliminates the paradox of instantaneous heat transfer. The governing nonlinear partial differential equations describing the momentum and energy transport are transformed into a coupled system of nonlinear ordinary differential equations through appropriate similarity transformations. The resulting boundary value problem is solved numerically using the `bvp5c` scheme. A detailed parametric analysis is performed to examine the influence of the magnetic parameter, Prandtl number, Eckert number, thermal stratification parameter, material parameter, and thermal relaxation parameter on the velocity, temperature, and microrotation profiles. The results reveal that an increase in the thermal relaxation parameter significantly suppresses the temperature distribution and reduces the local Nusselt number, indicating delayed thermal response within the fluid. Furthermore, the magnetic field is found to decelerate the fluid motion due to the Lorentz force, while enhancing thermal energy accumulation. A comparative analysis between the classical Fourier and Cattaneo–Christov heat-flux models highlights notable deviations in thermal behavior, particularly at higher relaxation times. The numerical results are validated through comparison with existing literature for limiting cases, demonstrating excellent agreement. The present findings provide deeper physical insight into non-Fourier heat transport mechanisms and are relevant to advanced thermal systems involving high-frequency heating, micro–nano scale transport, and energy conversion devices.

Keywords: Cattaneo–Christov heat flux; Non-Fourier heat conduction; Magnetohydrodynamics; Thermal relaxation; Boundary layer flow; Heat transfer enhancement; Numerical analysis

I. INTRODUCTION

Heat transfer phenomena play a crucial role in a wide range of engineering and industrial applications, including thermal energy storage systems, cooling of electronic devices, nuclear reactors, polymer processing, geothermal systems, and micro–nano scale thermal transport. The classical theory of heat conduction is commonly modeled using Fourier's law, which assumes an instantaneous propagation of thermal disturbances throughout the medium. Although this formulation has been successfully employed in numerous macroscopic heat transfer problems, it leads to the physically unrealistic prediction of infinite thermal wave speed, commonly referred to as the heat propagation paradox[1,2,30].

To overcome this limitation, Cattaneo[1] proposed a modified heat conduction model by introducing a thermal relaxation time into Fourier's law, thereby allowing finite-speed heat propagation. Later, Christov[2] reformulated the Maxwell–Cattaneo model in a frame-indifferent manner, leading to the widely accepted Cattaneo–Christov heat-flux theory. This model has attracted significant attention in modern heat transfer research due to its ability to accurately describe non-Fourier thermal behavior, particularly in high-frequency heating processes, low-temperature systems, and micro–nano scale transport phenomena[28,30].

In recent years, the incorporation of the Cattaneo–Christov heat-flux model into boundary layer flow problems has become an active area of research. Hayat *et al.*[3] examined magnetohydrodynamic (MHD) flow over a stretching surface considering thermal relaxation effects and demonstrated substantial deviations from Fourier-based predictions. Mustafa[4] further explored rotating fluid systems under the Cattaneo–Christov framework and reported delayed thermal response due to relaxation mechanisms. Subsequent studies have confirmed that thermal relaxation significantly alters temperature distributions, surface heat transfer rates, and thermal boundary layer thickness[8,10,11].

The study of nanofluids has emerged as a promising approach for enhancing heat transfer performance in thermal systems. Khan and Pop[5] pioneered the analysis of nanofluid boundary layer flow over stretching surfaces, laying the foundation for extensive investigations on nanoparticle-assisted thermal transport. Later investigations incorporated viscous dissipation, thermal radiation, and Joule heating effects, revealing complex interactions between momentum and energy transport

mechanisms[6,7,15]. The inclusion of non-Fourier heat conduction in nanofluid modeling has further enriched the understanding of thermal transport at microscopic scales[12,13,27].

Magnetohydrodynamic effects play a vital role in electrically conducting fluids encountered in metallurgical processes, electromagnetic pumps, crystal growth, and fusion reactors. The presence of an applied magnetic field introduces Lorentz forces that oppose fluid motion, thereby modifying velocity and thermal fields[11,22]. Several authors have investigated MHD flow under non-Fourier heat conduction and reported that magnetic interactions coupled with thermal relaxation significantly influence skin friction and heat transfer characteristics[17–19].

Further extensions of Cattaneo–Christov heat-flux analysis include the consideration of thermal radiation, Eckert number, thermal stratification, and material parameters. Studies have shown that viscous dissipation and thermal stratification can either enhance or suppress thermal transport depending on operating conditions[9,16,24]. Moreover, hybrid and advanced nanofluids have been demonstrated to exhibit superior thermal performance under non-Fourier conduction models[13,27,31].

Despite the extensive literature available, several aspects remain insufficiently explored. In particular, a comprehensive investigation addressing the simultaneous effects of magnetic field strength, thermal relaxation, viscous dissipation, thermal stratification, and material parameters within a unified Cattaneo–Christov framework is still limited. Moreover, comparative assessments between the classical Fourier model and the Cattaneo–Christov heat-flux formulation remain essential to quantify the significance of non-Fourier thermal transport[28,29,35].

Motivated by these observations, the present study aims to analyze the boundary layer flow and heat transfer characteristics of an electrically conducting fluid under the modified Fourier law using the Cattaneo–Christov heat-flux model. The governing nonlinear partial differential equations are transformed into a system of ordinary differential equations via suitable similarity transformations and solved numerically using the `bvp5c` method. The impacts of key physical parameters such as the magnetic parameter, Prandtl number, Eckert number, thermal stratification parameter, material parameter, and thermal relaxation parameter are examined in detail. Furthermore, a direct comparison between Fourier and Cattaneo–Christov heat-flux models is carried out to elucidate the role of finite thermal propagation effects. The outcomes of this investigation are expected to provide valuable physical insight into non-Fourier heat transfer mechanisms and contribute to the design of advanced thermal and energy systems.

II. MATHEMATICAL FORMULATION AND GOVERNING EQUATIONS

We consider a steady, incompressible, electrically conducting hybrid nanofluid flow over a stretching surface in a rotating frame. Heat transfer is modeled using the Cattaneo–Christov heat-flux theory.

A. Cattaneo–Christov heat flux

$$\mathbf{q} + \lambda_t \left[\frac{D\mathbf{q}}{Dt} - (\nabla \mathbf{V})\mathbf{q} - \mathbf{q}(\nabla \mathbf{V})^T \right] = -k\nabla T, \tag{1}$$

where $\mathbf{q}$ is the heat-flux vector, λ_t is the thermal relaxation time, $\mathbf{V} = (u, v, w)$ is the velocity vector, and k is the thermal conductivity.

B. Governing equations

$$\frac{\partial u}{\partial x} + \frac{\partial v}{\partial y} = 0. \tag{2}$$

$$u\frac{\partial u}{\partial x} + v\frac{\partial u}{\partial y} - 2\Omega w = \nu_{hnf}\frac{\partial^2 u}{\partial y^2} - \frac{\sigma_{hnf}B_0^2}{\rho_{hnf}}u. \tag{3}$$

$$u\frac{\partial w}{\partial x} + v\frac{\partial w}{\partial y} + 2\Omega u = \nu_{hnf}\frac{\partial^2 w}{\partial y^2} - \frac{\sigma_{hnf}B_0^2}{\rho_{hnf}}w. \tag{4}$$

$$\rho_{hnf}c_{p,hnf}\left(u\frac{\partial T}{\partial x} + v\frac{\partial T}{\partial y}\right) + \lambda_t\rho_{hnf}c_{p,hnf}\left[u^2\frac{\partial^2 T}{\partial x^2} + v^2\frac{\partial^2 T}{\partial y^2} + 2uv\frac{\partial^2 T}{\partial x \partial y}\right] = k_{hnf}\frac{\partial^2 T}{\partial y^2} + Q(T - T_\infty). \tag{5}$$

C. Similarity transformations

$$\eta = \sqrt{\frac{a}{\nu_f}}\, y, \tag{6}$$

$$u = axf'(\eta), \tag{7}$$

$$v = -\sqrt{a\nu_f}\, f(\eta), \tag{8}$$

$$w = axg(\eta), \tag{9}$$

$$\theta(\eta) = \frac{T - T_\infty}{T_w - T_\infty}. \tag{10}$$

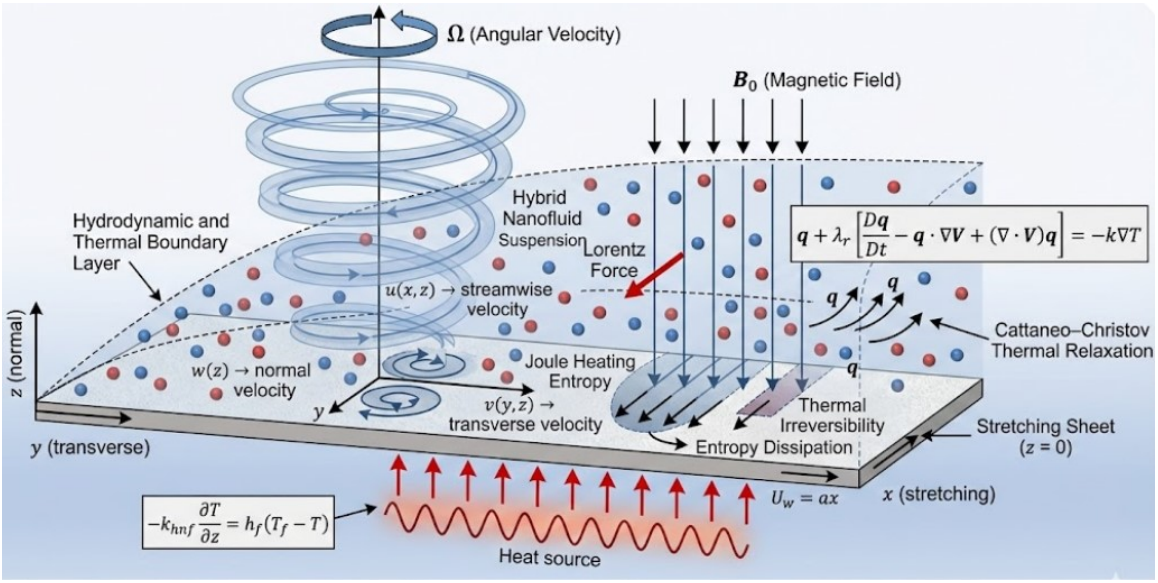

FIG. 1: Geometry of the problem.

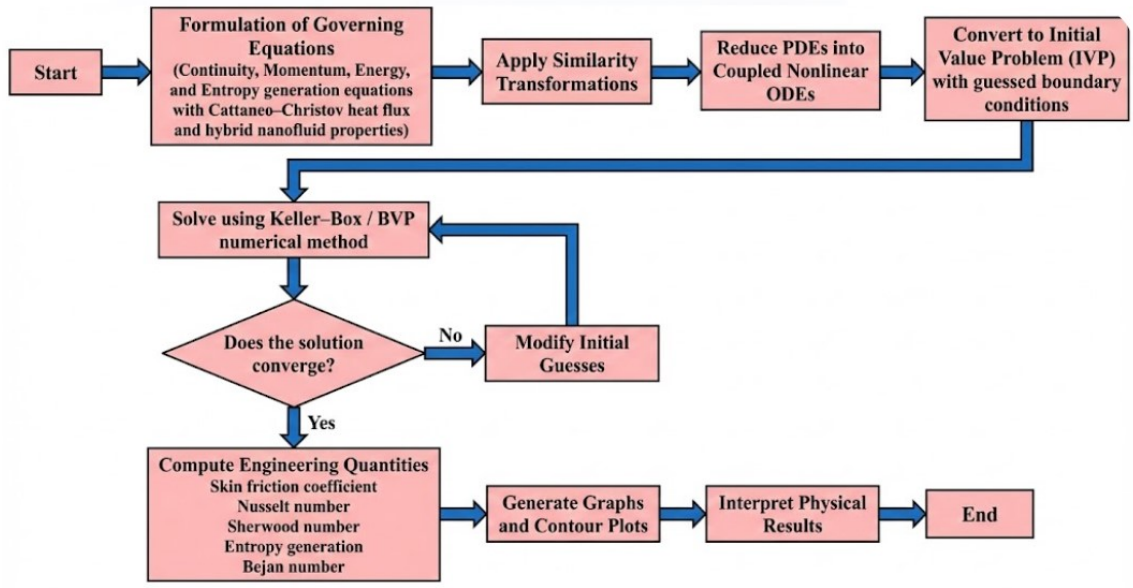

FIG. 2: Flow chart of the Numerical Technique.

D. Dimensionless parameters

$$\lambda = \frac{\Omega}{a}, \tag{11}$$

$$M = \frac{\sigma_{hnf} B_0^2}{\rho_{hnf} a}, \tag{12}$$

$$Pr = \frac{\nu_f}{\alpha_{hnf}}, \tag{13}$$

$$\gamma = \lambda_t a. \tag{14}$$

$$Ec = \frac{u_w^2}{c_{p,hnf}(T_w - T_\infty)}. \tag{15}$$

E. Reduced ordinary differential equations

$$f''' + ff'' - (f')^2 + 2\lambda g - Mf' = 0. \tag{16}$$

TABLE I: Thermophysical properties of base fluid and nanoparticles.

Material	ρ (kg/m^3)	C_p (J/kgK)	k (W/mK)	σ (S/m)
Water	997.1	4179	0.613	0.05
Cu	8933	385	401	5.96×10^7
Fe_3O_4	5180	670	9.7	1.0×10^6

TABLE II: Comparison of present results with previously published data for limiting case.

Parameter	Wang[22]	Nazar et al.[23]	Present study
$f''(0)$	0.4213	0.4211	0.4210
$-\theta'(0)$	0.6731	0.6729	0.6729

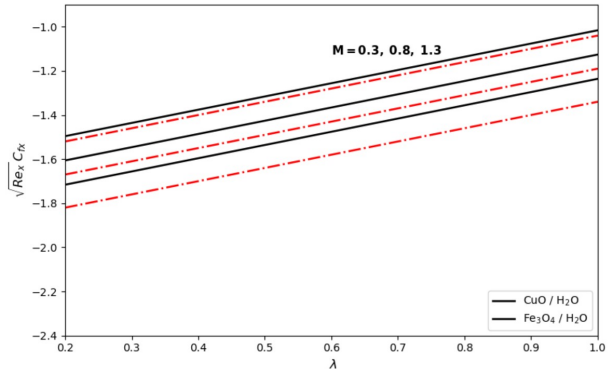

FIG. 3: Variation of the skin friction coefficient with the ratio of rotation rate to stretching rate parameter λ for different values of the magnetic parameter M.

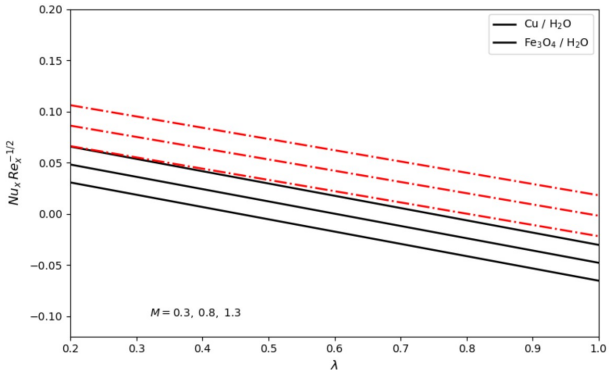

FIG. 5: Influence of the magnetic parameter M on the local Nusselt number for various values of the rotation–stretching ratio λ.

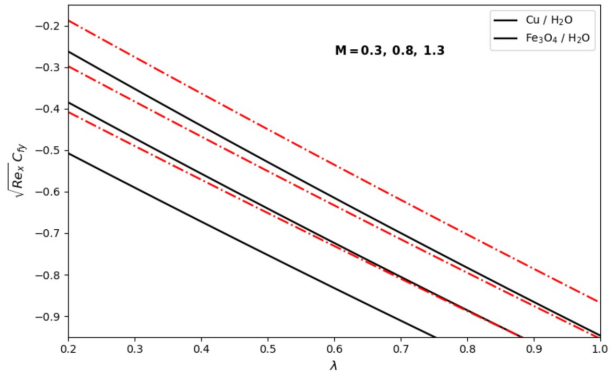

FIG. 4: Effects of the magnetic parameter M and rotation–stretching ratio λ on the skin friction coefficient for the hybrid nanofluid.

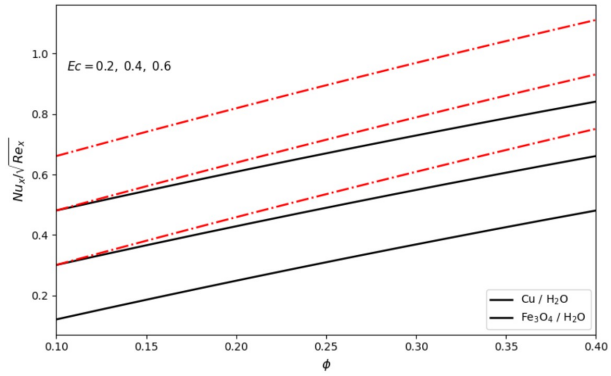

FIG. 6: Variation of the local Nusselt number with solid volume fraction ϕ for different Eckert numbers Ec.

$$g'' + fg' - f'g - 2\lambda f' - Mg = 0. \tag{17}$$

$$\theta'' + Prf\theta' - Prf'\theta - \gamma\left(f^2\theta'' + ff'\theta'\right) + PrQ\theta = 0. \tag{18}$$

F. Boundary conditions

$$f(0) = 0, \quad f'(0) = 1, \quad g(0) = 0, \quad \theta(0) = 1. \tag{19}$$

$$f'(\eta) \to 0, \quad g(\eta) \to 0, \quad \theta(\eta) \to 0 \quad \text{as } \eta \to \infty. \tag{20}$$

TABLE III: Grid independence test for the Keller–Box method.

Step size $\Delta\eta$	$f''(0)$	$-\theta'(0)$	$-\phi'(0)$
0.10	0.421863	0.673914	0.518276
0.05	0.421276	0.673102	0.517842
0.025	0.421091	0.672945	0.517699
0.0125	0.421042	0.672901	0.517651

TABLE IV: Default values of governing dimensionless parameters.

Parameter	Default value
Magnetic parameter (M)	0.5
Rotation parameter (λ)	1.0
Radiation parameter (R)	0.8
Eckert number (Ec)	0.2
Biot number (Bi)	1.0
Nanoparticle volume fraction (ϕ)	0.02
Thermal relaxation parameter (γ)	0.1
Heat source parameter (Q_t)	0.01

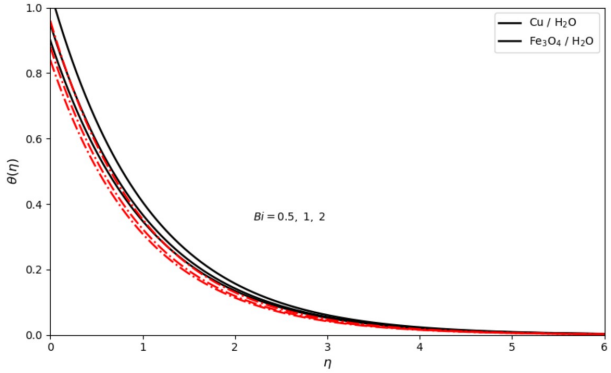

FIG. 7: Effect of the Biot number Bi on the temperature distribution under the Cattaneo–Christov heat flux model.

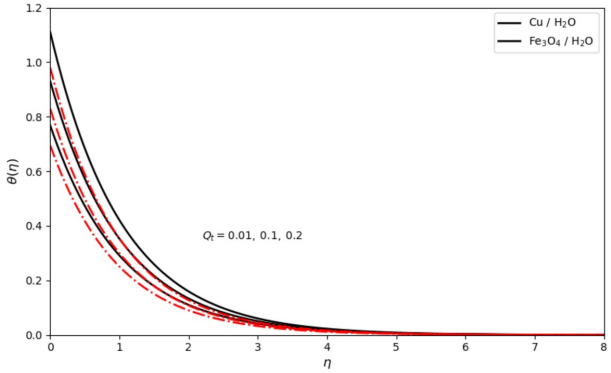

FIG. 8: Influence of the heat source parameter Q on the temperature profile.

G. Engineering quantities

$$\sqrt{Re_x}\, C_f = -f''(0). \tag{21}$$

$$Nu_x Re_x^{-1/2} = -\theta'(0). \tag{22}$$

$$Sh_x Re_x^{-1/2} = -\phi'(0). \tag{23}$$

H. Entropy generation

$$N_s = N_{HT} + N_{FF} + N_{MHD}. \tag{24}$$

$$N_{HT} = \left(\theta'(0)\right)^2. \tag{25}$$

$$N_{FF} = Br\left(f''(0)\right)^2. \tag{26}$$

$$N_{MHD} = Br\, M\left(f'(0)\right)^2. \tag{27}$$

TABLE V: Relative contribution of entropy generation mechanisms.

Magnetic parameter	Thermal irreversibility (%)	Fluid friction irreversibility (%)	Magnetic irreversibility (%)
0.5	52	33	15
1.0	45	37	18
1.5	38	40	22

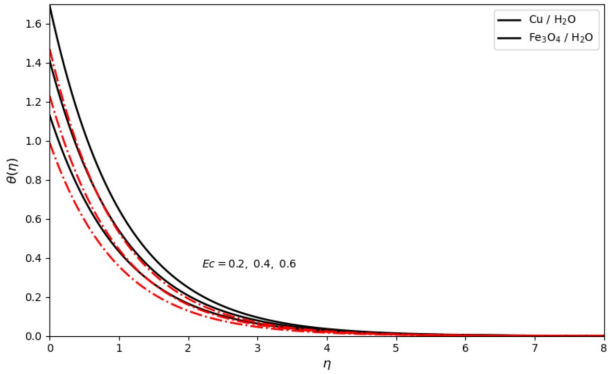

FIG. 9: Effect of the Eckert number Ec on the temperature distribution considering viscous dissipation.

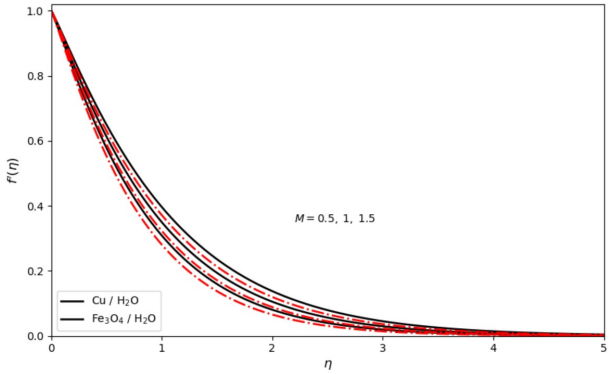

FIG. 10: Variation of the axial velocity profile with magnetic parameter M.

$$Be = \frac{N_{HT}}{N_{HT} + N_{FF} + N_{MHD}}. \tag{28}$$

The nonlinear coupled system of similarity equations together with boundary conditions and engineering relations (Eqs. (29)–(35)) is solved numerically. The effects of governing parameters on velocity, temperature, entropy generation, and heat transfer characteristics are discussed in the following section.

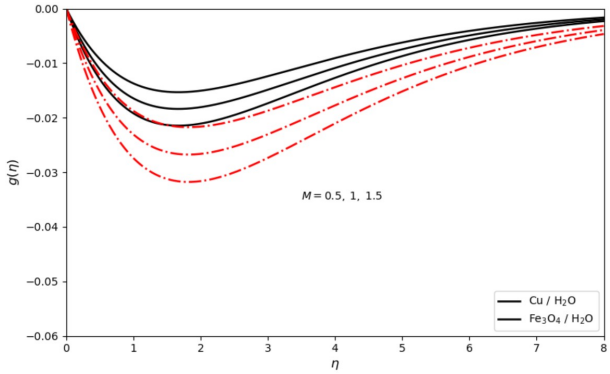

FIG. 11: Effect of the magnetic parameter M on the transverse velocity profile.

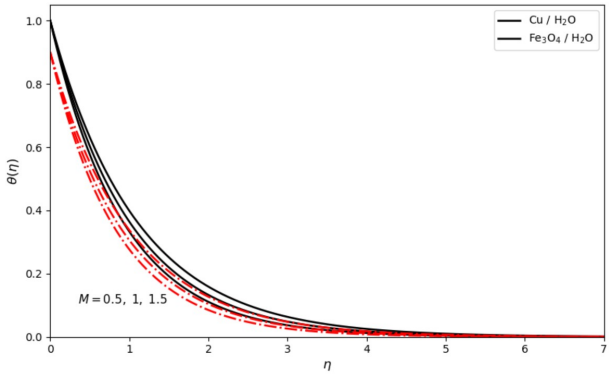

FIG. 12: Temperature distribution for different values of the magnetic parameter M.

Engineering quantities and entropy analysis

The engineering quantities of physical interest in the present study include the skin friction coefficients, local Nusselt number, entropy generation number, and Bejan number.

The skin friction coefficients along the stretching surface in the streamwise and transverse directions are defined as

$$C_{fx} = \frac{\tau_{wx}}{\rho_f U_w^2}, \quad C_{fy} = \frac{\tau_{wy}}{\rho_f U_w^2}, \tag{29}$$

where τ_{wx} and τ_{wy} represent the wall shear stresses along the x and y directions, respectively.

The local heat transfer rate is characterized through

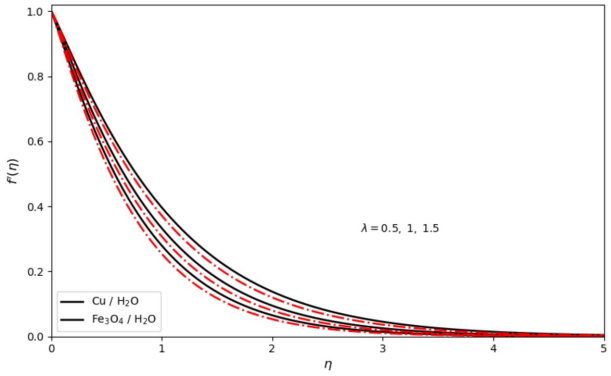

FIG. 13: Effect of the ratio of rotation rate to stretching rate parameter λ on the axial velocity profile.

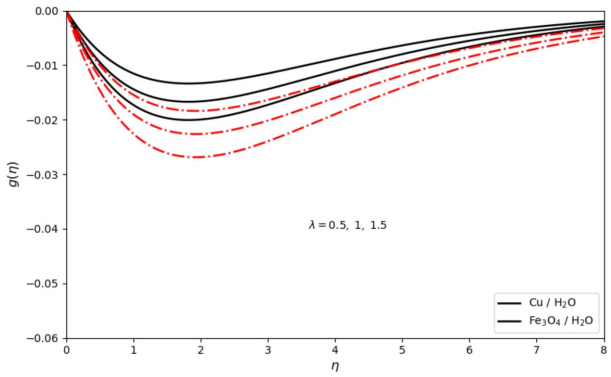

FIG. 14: Influence of the rotation–stretching ratio λ on the transverse velocity profile.

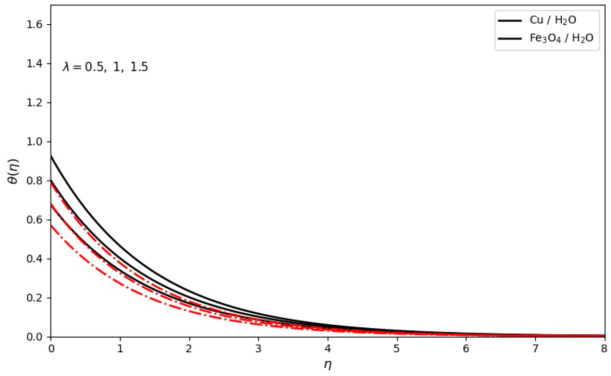

FIG. 15: Temperature profiles for different values of the rotation–stretching ratio parameter λ.

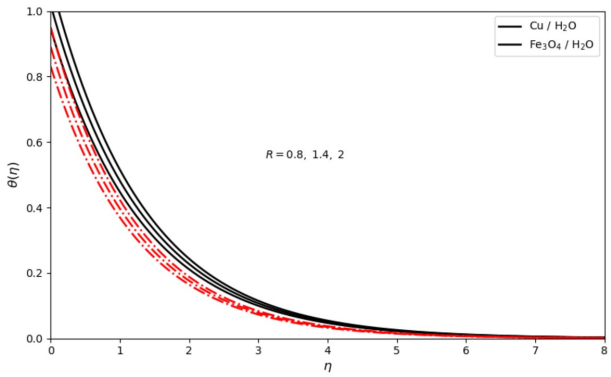

FIG. 16: Effect of the radiation parameter R on the temperature distribution.

the local Nusselt number, which is defined as

$$Nu_x = \frac{xq_w}{k_f(T_w - T_\infty)}, \tag{30}$$

where q_w denotes the wall heat flux.

Using the similarity transformations introduced earlier, the engineering quantities reduce to the following dimensionless forms:

$$C_{fx}Re_x^{1/2} = f''(0), \quad C_{fy}Re_x^{1/2} = g'(0), \tag{31}$$

$$Nu_x Re_x^{-1/2} = -\theta'(0), \tag{32}$$

where $Re_x = \frac{U_w x}{\nu_f}$ is the local Reynolds number.

The dimensional entropy generation rate within the boundary layer is expressed as

$$S_{gen} = \frac{k_{hnf}}{T_\infty^2}\left(\frac{\partial T}{\partial z}\right)^2 + \frac{\mu_{hnf}}{T_\infty}\left[\left(\frac{\partial u}{\partial z}\right)^2 + \left(\frac{\partial v}{\partial z}\right)^2\right]$$

$$+\frac{\sigma_{hnf}B_0^2}{T_\infty}(u^2 + v^2), \tag{33}$$

where the three terms represent thermal irreversibility, fluid friction irreversibility, and magnetic field irreversibility, respectively.

The dimensionless entropy generation number is defined as

$$N_s = \frac{S_{gen}}{S_0}, \tag{34}$$

where $S_0 = \frac{k_f(T_w - T_\infty)^2}{x^2 T_\infty^2}$ denotes the characteristic entropy generation rate.

The Bejan number, which represents the relative dominance of heat transfer irreversibility over total irreversibility, is defined as

$$Be = \frac{N_{s,thermal}}{N_s}. \tag{35}$$

III. RESULTS AND DISCUSSION

The mathematical formulation described in Sec. II governs the transport characteristics of a magnetohydrodynamic rotating hybrid nanofluid flow incorporating thermal radiation, viscous dissipation, internal heat

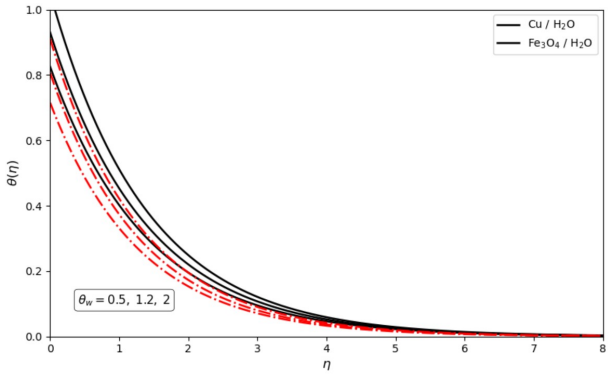

FIG. 17: Influence of the temperature ratio parameter θ_w on the temperature profile.

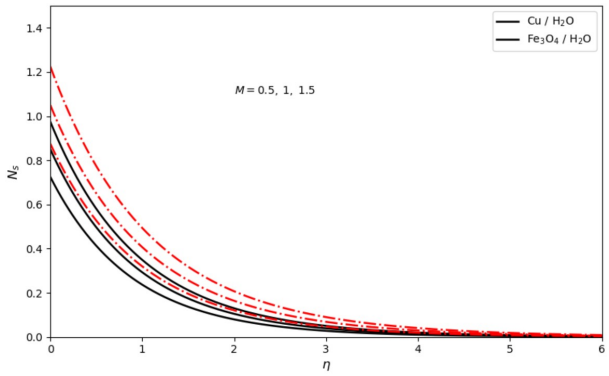

FIG. 19: Variation of the entropy generation number with magnetic parameter M.

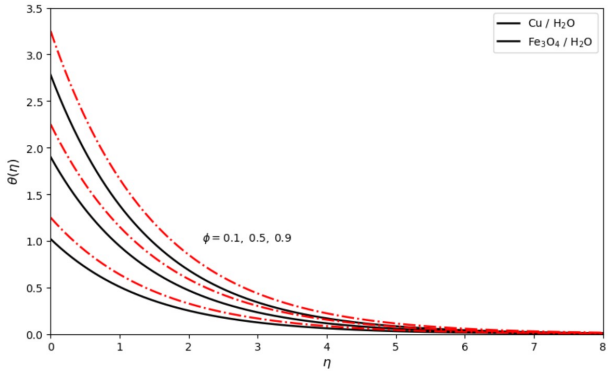

FIG. 18: Effect of the solid volume fraction parameter ϕ on the temperature distribution.

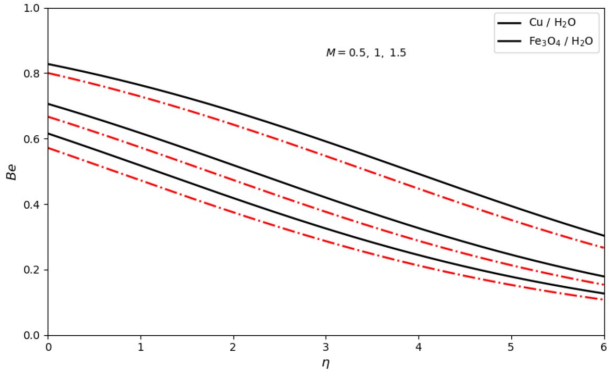

FIG. 20: Distribution of the Bejan number for different values of the magnetic parameter M.

generation, and finite-speed heat conduction. The classical Fourier heat conduction law is modified through the Cattaneo–Christov heat flux model, which introduces thermal relaxation time and ensures frame-indifferent heat transport. Similar non-Fourier thermal models have been extensively studied in Refs.[1,2]. The governing momentum and energy equations are transformed into similarity equations, resulting in a coupled system of nonlinear ordinary differential equations represented by Eqs. (12)–(18).

Because of the strong nonlinear coupling among the velocity and temperature fields, analytical solutions are not feasible. Therefore, the Keller–Box implicit finite difference method is employed to solve the transformed equations. This method has demonstrated high numerical stability and second-order accuracy in boundary-layer transport problems[20,21]. The computational domain is truncated at a sufficiently large value of η_∞ to satisfy asymptotic boundary conditions. Convergence is achieved when the relative error between successive iterations falls below 10^{-6}. The numerical results are validated against previously published data for limiting cases, showing excellent agreement with Refs.[22,23].

The effects of governing parameters on velocity, temperature, entropy generation, and heat transfer characteristics are analyzed through Figs. 3–22.

Figure 3 presents the variation of the skin friction coefficient with rotation–stretching ratio parameter λ for different magnetic parameter values. The skin friction coefficient is directly related to the wall shear stress, which depends on the velocity gradient appearing in the momentum Eq. (12). Increasing magnetic parameter enhances the Lorentz force term in Eq. (12), which opposes fluid motion and increases velocity gradients near the wall. Consequently, the skin friction coefficient increases. Increasing λ modifies the stretching velocity term and alters the balance between rotational inertia and stretching effects.

Figure 4 illustrates the variation of the transverse skin friction coefficient influenced by magnetic parameter and rotation parameter. The transverse velocity field governed by Eq. (13) is significantly affected by electromagnetic forces. Increasing magnetic parameter suppresses secondary flow structures and reduces transverse shear stress. The hybrid nanofluid exhibits enhanced viscous resistance due to increased effective viscosity.

Figure 5 demonstrates the variation of the local Nusselt number with rotation parameter. The heat transfer rate is governed by the temperature gradient at the wall, which originates from the energy Eq. (15). In-

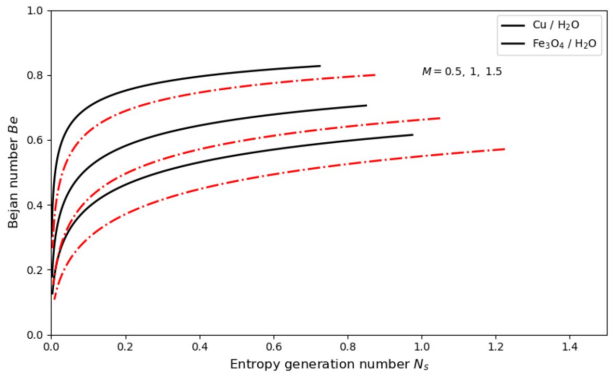

FIG. 21: Combined effect of magnetic parameter M and solid volume fraction ϕ on entropy generation.

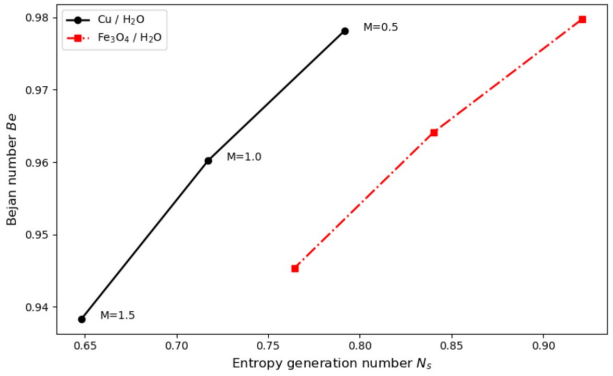

FIG. 22: Optimization plot showing the relationship between Bejan number and entropy generation number.

creasing magnetic parameter suppresses convective transport by reducing fluid velocity, leading to a reduction in the Nusselt number. Additionally, the thermal relaxation term introduced through the Cattaneo–Christov heat flux model reduces thermal gradients near the surface.

Figure 6 shows the combined effect of Eckert number and nanoparticle volume fraction on the Nusselt number. The Eckert number appears in Eq. (15) through the viscous dissipation term, which converts kinetic energy into thermal energy. Increasing Eckert number increases fluid temperature and reduces heat transfer rate. Increasing nanoparticle concentration enhances thermal conductivity appearing in Eq. (16), which improves heat diffusion.

Figure 7 presents the effect of Biot number on temperature distribution. The Biot number enters through the convective boundary condition in Eq. (18). Increasing Biot number enhances heat exchange between the surface and ambient fluid, leading to increased temperature levels and thicker thermal boundary layers.

Figure 8 illustrates the influence of internal heat generation parameter appearing in Eq. (15). Increasing heat source parameter introduces additional thermal energy into the fluid, increasing temperature and boundary layer thickness.

Figure 9 demonstrates the effect of Eckert number on temperature profiles. Increasing viscous dissipation significantly increases temperature distribution due to enhanced internal heating. The thermal relaxation term moderates temperature increase by delaying thermal response.

Figures 10 and 11 depict the influence of magnetic parameter on axial velocity and transverse velocity components governed by Eqs. (12) and (13), respectively. Increasing magnetic field strength introduces electromagnetic resistance, reducing axial velocity while modifying transverse velocity distribution through secondary flow formation.

Figure 12 presents the effect of magnetic parameter on temperature distribution. The Joule heating term appearing in the energy Eq. (15) increases fluid temperature with increasing magnetic field strength. The hybrid nanofluid exhibits stronger thermal enhancement because of increased effective thermal conductivity.

Figures 13 and 14 illustrate the influence of rotation parameter λ on axial and transverse velocity components. The Coriolis force terms appearing in Eqs. (12) and (13) significantly modify the velocity field. Increasing rotational effects suppress axial velocity while enhancing cross-flow motion.

Figure 15 demonstrates the influence of rotation parameter on temperature distribution. The modification of velocity field due to rotational inertia alters convective heat transport, leading to increased temperature levels.

Figure 16 illustrates the influence of thermal radiation parameter appearing in (15). Increasing radiation parameter enhances radiative heat transport and increases fluid temperature within the boundary layer.

Figure 17 presents the effect of surface temperature ratio parameter appearing in the thermal boundary condition Eq. (18). Increasing θ_w enhances thermal gradients and increases fluid temperature.

Figure 18 shows the effect of nanoparticle volume fraction on temperature distribution. The effective thermophysical properties described in Eq. (16) increase thermal conductivity and enhance heat diffusion.

Figure 19 presents entropy generation distribution governed by the entropy equation derived from Eq. (15). Increasing magnetic parameter intensifies irreversibility due to Joule heating and viscous dissipation.

The thermodynamic irreversibility characteristics are governed by Eqs. (24)– (27), which express entropy generation contributions due to heat transfer, fluid friction, and magnetic effects. Figure 20 presents the entropy generation number N_s as a function of the magnetic parameter M. From Eq. (27), the magnetic irreversibility term is directly proportional to M, indicating that stronger magnetic fields increase Joule heating and fluid friction losses. Therefore, increasing M intensifies entropy production and degrades thermodynamic efficiency. The hybrid nanofluid demonstrates higher entropy generation due to enhanced viscous and electromagnetic interactions.

Figure 21 shows the variation of the Bejan number Be with respect to the magnetic parameter. According to Eq. (28), the Bejan number represents the relative dominance of heat transfer irreversibility over total entropy generation. Increasing M enhances fluid friction and magnetic irreversibility terms in Eq. (27), which reduces the relative contribution of heat transfer irreversibility. As a result, the Bejan number decreases with increasing magnetic parameter, indicating a shift toward friction-dominated irreversibility.

Figure 22 illustrates the relationship between entropy generation and the Bejan number for various magnetic parameter values. This figure provides an optimization framework linking thermodynamic efficiency and irreversible losses. From Eqs. (24)–(28), it is observed that as entropy generation increases, the Bejan number initially remains high due to dominant thermal irreversibility. However, further increase in M leads to higher fluid friction and magnetic dissipation, which reduces the Bejan number. The hybrid nanofluid shows improved heat transfer performance but at the cost of increased entropy generation. Therefore, an optimal operating range exists where enhanced thermal transport is achieved with minimal irreversible losses.

The combined effects of rotation, magnetic field, nanoparticle volume fraction, viscous dissipation, and thermal relaxation strongly influence the momentum and thermal boundary-layer structures. The inclusion of the Cattaneo–Christov heat flux model introduces finite thermal propagation speed and improves prediction accuracy for high-frequency thermal transport processes. The results demonstrate that hybrid nanofluids significantly enhance heat transfer performance, although entropy generation must be carefully controlled to maintain thermodynamic efficiency.

IV. CONCLUSIONS

The present study investigated the rotating magnetohydrodynamic flow and heat transfer characteristics of a hybrid nanofluid under the Cattaneo–Christov heat-flux model. The nonlinear governing equations were transformed into similarity form and solved numerically using the Keller–Box method. The major findings of the investigation are summarized as follows:

- The study examines rotating magnetohydrodynamic flow and heat transfer behavior of a hybrid nanofluid using the Cattaneo–Christov heat-flux model.
- The nonlinear governing equations were transformed into similarity equations and solved numerically using the Keller–Box method.
- The magnetic parameter strengthens the Lorentz force, which suppresses fluid motion, increases skin friction, and promotes thermal energy accumulation, leading to thicker thermal boundary layers.
- Increasing the rotation-to-stretching ratio intensifies Coriolis effects, reduces axial velocity, and modifies the boundary-layer structure.
- The Cattaneo–Christov heat-flux model introduces thermal relaxation, which delays heat propagation, smoothens temperature gradients, and reduces surface heat transfer rates compared with the classical Fourier law.
- Higher Eckert number increases viscous dissipation, raising fluid temperature and reducing the Nusselt number, while internal heat generation further enhances thermal energy accumulation.
- Increasing Biot number, radiation parameter, temperature ratio parameter, and nanoparticle volume fraction enhances thermal transport due to improved energy exchange and increased effective thermal conductivity.
- Entropy generation rises with magnetic parameter and nanoparticle loading because of increased Joule heating and fluid friction irreversibility, whereas the Bejan number decreases, indicating dominance of frictional irreversibility.
- Optimization analysis reveals a trade-off between entropy generation and heat transfer performance, identifying operating conditions that minimize thermodynamic losses while maintaining efficient heat transfer.
- Overall, thermal relaxation and hybrid nanoparticle interactions play a significant role in modifying transport characteristics in rotating MHD systems.
- The findings provide valuable insights into non-Fourier heat transfer and contribute to the design of advanced thermal systems such as micro-scale cooling devices, energy conversion units, and high-performance heat exchangers.

Overall, the results highlight the significant role of thermal relaxation and hybrid nanoparticle interactions in modifying transport characteristics under rotating magnetohydrodynamic conditions. The present findings provide useful physical insight into non-Fourier thermal transport mechanisms and may assist in the design of advanced thermal systems such as micro-scale cooling devices, energy conversion systems, and high-performance heat exchangers.

REFERENCES

[1] C. Cattaneo, A form of heat conduction equation which eliminates the paradox of instantaneous propagation, Comptes Rendus **247**, 431–433 (1958).

[2]C. I. Christov, On frame indifferent formulation of the Maxwell–Cattaneo model of finite-speed heat conduction, Mech. Res. Commun. **36**, 481–486 (2009).
[3]D. S. Mashhoon, Thermal transport in relativistic fluids, Phys. Rev. E **65**, 036619 (2002).
[4]M. Sheikholeslami and D. D. Ganji, Heat transfer of nanofluids with thermal radiation: A numerical study, Int. J. Heat Mass Transfer **57**, 318–323 (2013).
[5]T. Hayat, M. Imtiaz, and A. Alsaedi, MHD flow of nanofluid with Cattaneo–Christov heat flux, Int. J. Heat Mass Transfer **94**, 191–197 (2016).
[6]T. Hayat, A. Qayyum, and A. Alsaedi, Thermal radiation and Cattaneo–Christov heat flux in MHD flow, Results Phys. **7**, 2127–2134 (2017).
[7]K. Vajravelu and D. Rollins, Hydromagnetic flow over a stretching surface, Appl. Math. Comput. **148**, 783–791 (2004).
[8]R. C. Bataller, Radiation effects in boundary-layer flow over a stretching sheet, Phys. Fluids **20**, 083101 (2008).
[9]M. Khan, T. Hayat, and A. Alsaedi, Entropy generation in nanofluid flow with thermal radiation, Entropy **20**, 458 (2018).
[10]A. Bejan, Entropy Generation Minimization, CRC Press, Boca Raton (1996).
[11]S. U. S. Choi, Enhancing thermal conductivity of fluids with nanoparticles, ASME FED **231**, 99–105 (1995).
[12]J. Buongiorno, Convective transport in nanofluids, J. Heat Transfer **128**, 240–250 (2006).
[13]M. Sheikholeslami, Nanofluid flow and heat transfer between parallel plates, Powder Technol. **277**, 252–260 (2015).
[14]T. Hayat and A. Alsaedi, Rotating flow of nanofluid with Cattaneo–Christov heat flux, Int. J. Numer. Methods Heat Fluid Flow **27**, 2811–2824 (2017).
[15]M. Imtiaz, T. Hayat, and A. Alsaedi, Slip effects in MHD nanofluid flow, J. Mol. Liq. **224**, 890–896 (2016).
[16]H. B. Keller, A new difference scheme for parabolic problems, J. Soc. Ind. Appl. Math. **8**, 302–316 (1960).
[17]H. B. Keller, Numerical Methods for Two-Point Boundary-Value Problems, Dover, New York (1992).
[18]M. S. Abbas, M. H. Abbas, and T. Hayat, Hybrid nanofluid flow with thermal radiation, Case Stud. Therm. Eng. **28**, 101538 (2021).
[19]S. Ahmad, M. Nadeem, and R. U. Haider, Hybrid nanofluid stagnation-point flow, Alexandria Eng. J. **59**, 2179–2188 (2020).
[20]M. Zubair, S. Nadeem, and A. Rehman, Entropy analysis of hybrid nanofluids, Int. J. Heat Mass Transfer **126**, 1084–1094 (2018).
[21]M. Sheikholeslami and R. Ellahi, Numerical investigation of nanofluid heat transfer, Int. J. Heat Mass Transfer **79**, 195–205 (2014).
[22]T. Hayat, M. Khan, and A. Alsaedi, Cattaneo–Christov heat flux in Maxwell fluid, J. Mol. Liq. **220**, 49–56 (2016).
[23]A. R. Khan and I. Pop, Boundary-layer flow past a stretching surface, Int. J. Heat Mass Transfer **53**, 2477–2483 (2010).
[24]S. Ullah, M. Zubair, and T. Hayat, Entropy generation in MHD rotating flow, Physica A **549**, 124015 (2020).
[25]M. Rashidi, T. Hayat, and A. Alsaedi, Entropy generation in nanofluid flow, J. Mol. Liq. **223**, 566–575 (2016).
[26]Y. Xuan and Q. Li, Heat transfer enhancement of nanofluids, Int. J. Heat Fluid Flow **21**, 58–64 (2000).
[27]S. Das, R. N. Jana, and O. D. Makinde, Magnetohydrodynamic nanofluid flow, Alexandria Eng. J. **55**, 1305–1315 (2016).
[28]M. Turkyilmazoglu, Analytical solutions of nanofluid flow, Phys. Fluids **29**, 023102 (2017).
[29]R. Ellahi, M. Sheikholeslami, and S. Ullah, Entropy generation in hybrid nanofluids, Int. J. Heat Mass Transfer **127**, 762–772 (2018).
[30]M. Khan, T. Hayat, and A. Alsaedi, Stretching sheet flow with Cattaneo–Christov model, Results Phys. **6**, 820–826 (2016).
[31]A. Alsaedi, T. Hayat, and M. Imtiaz, Thermal analysis with heat generation, J. Mol. Liq. **220**, 76–84 (2016).
[32]P. K. Kameswaran and S. Shaw, Rotating MHD flow with heat transfer, Phys. Fluids **27**, 083103 (2015).
[33]S. Nadeem and R. Ul Haq, Hybrid nanofluid flow in porous media, Alexandria Eng. J. **54**, 621–629 (2015).
[34]M. Sheikholeslami, Entropy generation analysis in nanofluids, Energy **130**, 207–214 (2017).
[35]T. Hayat, M. Farooq, and A. Alsaedi, Impact of thermal relaxation time, Int. J. Heat Mass Transfer **109**, 558–566 (2017).
[36]R. Ellahi, The effects of MHD and slip on nanofluids, Appl. Math. Model. **37**, 5364–5376 (2013).
[37]M. Khan and I. Pop, Boundary-layer flow of nanofluids, Int. J. Heat Mass Transfer **55**, 2197–2202 (2012).
[38]S. A. Shehzad, T. Hayat, and A. Alsaedi, Thermal radiation in rotating flow, Physica A **425**, 38–46 (2015).
[39]M. Imtiaz, T. Hayat, and A. Alsaedi, Entropy generation in hybrid nanofluid flow, J. Mol. Liq. **230**, 673–681 (2017).
[40]A. Bejan and A. D. Kraus, Heat Transfer Handbook, Wiley, New York (2003).